JOURNAL OF THERMOPHYSICS AND HEAT TRANSFER
Vol. 23, No. 1, January–March 2009

Heat Conduction in Two-Dimensional Slabs Subjected to Spatially Decaying Laser Pulses

L. A. Peterson,* T. K. Cheung,† T. T. Lam,‡ and B. A. Blake§
The Aerospace Corporation, El Segundo, California

DOI: 10.2514/1.29986

The temperature distribution within a two-dimensional rectangular slab subjected to a time-varying and spatially decaying laser source is presented. Linear boundary conditions involving nonhomogeneities are considered in this study for two slab thicknesses. The solution of the nonhomogeneous and time-dependent heat conduction boundary-value problem is obtained with the integral-transform technique. The temperature results are presented for various thermal and geometric dimensionless parameters as well as two levels of laser power intensity. Additionally, the results are compared with one-dimensional analyses to examine the effect of in-plane heat spreading in a two-dimensional slab. The knowledge gained from this study will provide a better understanding of heat treatment manufacturing processes in microtechnology, where precise control of the location of the maximum temperature during laser-induced heating is required.

Nomenclature

a	=	function, $\alpha(\beta_m^2 + \gamma_n^2)$
b	=	function, $2\sqrt{2}/d$
Bi	=	Biot number, $h/\mu k$ or $hL/2k$
c_p	=	specific heat, J/kg · K
d	=	laser beam diameter, mm
$\mathrm{erf}(x)$	=	error function
$\bar{g}$	=	function, K/ns
$\dot{g}'''$	=	energy generation rate per unit volume, W/m^3
$\dot{g}(t)$	=	temporally decaying portion of the laser source
$\dot{g}(x)$	=	distribution of the laser source in the x direction
$\dot{g}(y)$	=	spatially decaying portion of the laser source in the y direction
H	=	ratio of convection heat transfer coefficient to thermal conductivity (h/k), m^{-1}
h	=	convective heat transfer coefficient, W/m^2 · K
i	=	imaginary unit
I_o	=	laser peak power density, W/m^2
k	=	thermal conductivity, W/m · K
L	=	thickness of the slab, m
M	=	normalization integral for the x direction, m
$m(\tau)$	=	temperature change with time
N	=	normalization integral for the y direction, m
n	=	real part of the refractive index
R	=	surface reflectivity
T	=	temperature, K
t	=	time, ns
T_∞	=	external environment temperature, K
T^*	=	temperature, $(T - T_\infty)/[I_o(1 - R)/\mu k]$
$T^*_{\max}$	=	maximum temperature within the slab
t'	=	dummy time variable for integration, ns
W	=	half width of the plate, m
X	=	eigenfunction for the x direction
x	=	x coordinate, m
x^*	=	distance, μx
x'	=	dummy spatial variable for integration, m
Y	=	eigenfunction for the y direction, m
y	=	y coordinate, m
y^*	=	distance, μy
y'	=	dummy spatial variable for integration, m
$y_{T^*_{\max}}$	=	value of y^* at maximum temperature
α	=	thermal diffusivity, $k/\rho c_p$, m^2/s
β	=	eigenvalue in the x direction, m^{-1}
γ	=	eigenvalue in the y direction, m^{-1}
Δ	=	difference
δ	=	laser pulse fall-time parameter, s^{-1}
θ	=	laser pulse rise-time parameter, s^{-1}
κ	=	imaginary part of the refractive index
λ	=	wavelength, nm
μ	=	absorption coefficient, m^{-1}
ρ	=	density, kg/m^3
τ	=	time, $t\alpha\mu^2$

Subscripts

m	=	index for the x direction
n	=	index for the y direction
1	=	incident surface, surface 1
1-D–2-D	=	difference between 1-D and 2-D calculations
2	=	nonincident surface, surface 2

Presented as Paper 0200 at the 45th Aerospace Sciences Meeting, Reno, NV, 8–11 January 2007; received 24 January 2007; revision received 27 August 2008; accepted for publication 14 September 2008.

*Member of Technical Staff, Spacecraft Thermal Department, Vehicle Systems Division, Engineering and Technology Group, P.O. Box 92957, Mail Stop M4/916.

†Senior Member of Technical Staff, Spacecraft Thermal Department, Vehicle Systems Division, Engineering and Technology Group, P.O. Box 92957, Mail Stop M4/916.

‡Director, Spacecraft Thermal Department, Vehicle Systems Division, Engineering and Technology Group, P.O. Box 92957, Mail Stop M4/908. Associate Fellow AIAA.

§Member of Technical Staff, Spacecraft Thermal Department, Vehicle Systems Division, Engineering and Technology Group; currently Lockheed Martin Space Systems Company, Sunnyvale, CA.

I. Introduction

LASERS have been widely used in the material processing industry for the heat treatment of metals and semiconductors [1,2]. An advantage of laser heating is that the incident beam can be carefully controlled to limit the heating to a small, localized area with temperature increases up to 108 K/s for a few nanoseconds to hundreds of milliseconds [2]. With this procedure thermally induced structural modifications can be confined within precisely controlled treatment zones.

Intense heating produced by laser incidence can adversely affect the integrity of solid structures due to the rapid degradation of material properties (e.g., optical, thermophysical properties, etc.),

Table 1 Laser pulse characteristics

	Wavelength, nm	I_o, maximum pulse peak power density, W/m^2	Pulse length, FWHM, ns	Beam diameter, d, mm	θ, 1/s	δ, 1/s
Laser 1	1000	1×10^{13}	25	1	4.9×10^7	2.45×10^8
Laser 2	1000	5×10^{12}	50	1	2.45×10^7	1.225×10^8

thermal distortion, phase change, and thermal diffusion. Dabby and Paek [3] stated that "explosive removal of material" could possibly occur when sufficient incident energy is absorbed within the solid. Blackwell [4] went further to explain that the phenomenon could be attributed to the cooling of the exposed surface while a localized temperature maximum existed within the material, thereby inducing an expanded phase change within the outer surface of the solid. It can be concluded that damage to materials caused by high-energy laser exposure is a strong function of material thermal response. Therefore, the accurate analysis of the thermal response constitutes an important element in assessing the overall reliability of solids subjected to high-power laser heating.

Several authors have presented closed-form solutions to one-dimensional heat conduction in a semi-infinite solid subjected to laser heating. Each study considered different definitions of the laser heating source function such as an exponentially (with position) decaying source (Blackwell [4], Chaudhry and Zubair [5]), a time-dependent source (Zubair and Chaudhry [6,7]), and a laser pulse (Yilbas [8]). All of these studies made use of the Laplace transform technique because they were limited to conduction in semi-infinite solids.

The purpose of this study is to investigate the heat conduction phenomenon in a two-dimensional slab subjected to time-varying and spatially decaying high-energy laser irradiation and non-homogeneous boundary conditions. This investigation is an extension of a recent paper published by Cheung et al. [9] for a one-dimensional finite slab in which a closed-form solution of the one-dimensional heat conduction problem using the integral-transform technique was obtained. In this study, the solution of the two-dimensional, nonhomogeneous, and time-dependent heat conduction problem will also be obtained using the same technique [10]. The thermal response within the material will be studied in detail with particular emphasis on the absorbed intensity of the laser source and surface cooling effects. The results will provide insight into the maximum temperature within the slab due to high-flux heating and cooling of the incident surface. Furthermore, results from this study will also be compared with a one-dimensional slab to examine the in-plane energy spreading effect on the temperature distribution for a two-dimensional slab.

II. Physical Problem Formulation

A schematic of a rectangular slab impinged by a spatially and temporally varying laser source is shown in Fig. 1 with imposed boundary conditions. It is assumed that the thermal and optical properties of the materials remain constant and that the slab thickness is uniform. In addition, the initial temperature field within the material is assumed to be uniform. At $t > 0$, a laser source, centered about $x = 0$, irradiates surface 1 with normal incidence. Based on the optical properties of the slab, the laser energy is partially reflected by the surface of the slab while the remaining energy is absorbed and conducted into the material. As the surface temperature rises above the temperature of the environment, heat is transferred to the environment by convection.

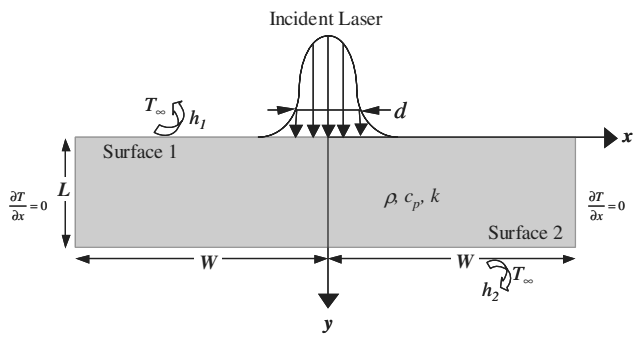

Fig. 1 Schematic diagram of a rectangular slab subjected to time-varying and spatially decaying laser irradiation.

An adiabatic boundary condition is applied at the axis of symmetry ($x = 0$), which allows for modeling of half of the laser beam. The Fourier heat transfer equation that governs a constant property, two-dimensional rectangular slab is given by

$$\frac{\partial^2 T(x,y,t)}{\partial x^2} + \frac{\partial^2 T(x,y,t)}{\partial y^2} + \frac{\dot{g}'''(x,y,t)}{k} = \frac{1}{\alpha}\frac{\partial T(x,y,t)}{\partial t} \tag{1}$$

The laser is modeled as a spatially and temporally varying energy source term as follows [11]:

$$\dot{g}'''(x,y,t) = I_o \mu (1-R)\dot{g}(x)\dot{g}(y)\dot{g}(t) \tag{2}$$

where

$$\dot{g}(x) = e^{-8x^2/d^2} \tag{3a}$$

$$\dot{g}(y) = e^{-\mu y} \tag{3b}$$

$$\dot{g}(t) = e^{-\theta t} - e^{-\delta t} \tag{3c}$$

The energy source term, Eq. (2), includes several functions as defined by Eq. (3) that specify the variation in intensity with respect to space and time. As is typical of many lasers (Ready [11]), it is suitable to assume the laser intensity has a Gaussian distribution, Eq. (3a). With respect to the variation in laser intensity in the through-thickness direction, Eq. (3b) captures the attenuation of the laser beam by the material. In terms of temporal variation, an exponential function designated by Eq. (3c) provides a pulse profile that accounts for the rise and fall times, making it more realistic than a step function or delta function. This exponential function is characterized by two pulse parameters θ and δ, which are provided in Table 1.

Based on the characteristics of solid state diode pumped lasers, the ratio of the pulse parameters is defined as $\theta/\delta = 1/5$ (Yilbas [8]). Surface reflectivity and absorption coefficients are optical properties of the slab dependent on the wavelength of the incident laser and can be, respectively, determined by the complex index of refraction as

$$R = \frac{(n-1)^2 + \kappa^2}{(n+1)^2 + \kappa^2} \tag{4}$$

$$\mu = \frac{4\pi\kappa}{\lambda} \tag{5}$$

The temporal function of the laser pulse is depicted in Fig. 2 while the spatial function of the laser pulse is shown in Fig. 3. Two different laser profiles (Fig. 2) were examined to demonstrate how the laser pulse parameters affect the slab. Both lasers have the same pulse parameter ratio, $\theta/\delta = 1/5$; however, the first laser (laser 1) has θ and δ values that are twice the magnitude of the second laser (laser 2). The full width at half-maximum (FWHM) pulse length of laser 2 is therefore twice as long as laser 1. The peak intensity of laser 1 is also twice as large as laser 2, making the total amount of energy deposited into the slab the same for both lasers. The temporal profile depicted in Fig. 2 is multiplied by the laser intensity to illustrate the area under

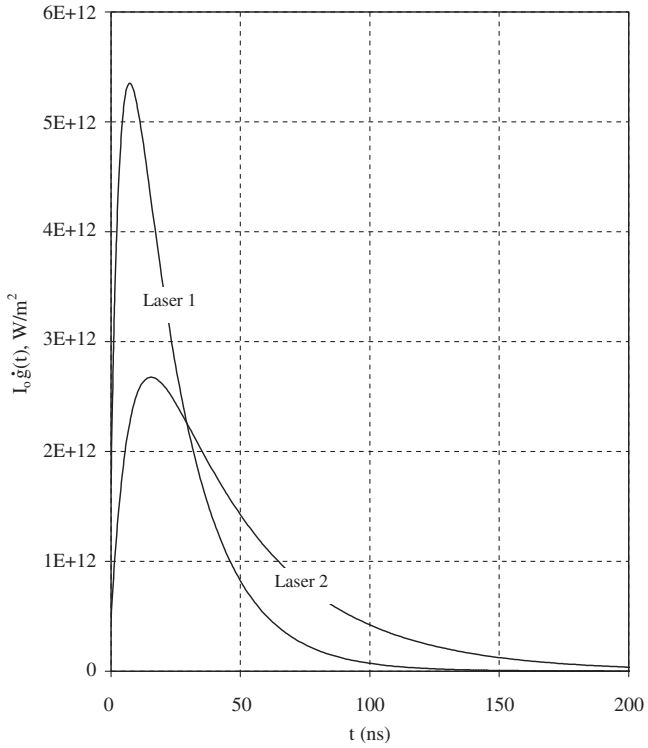

Fig. 2 Temporal function of the laser pulse.

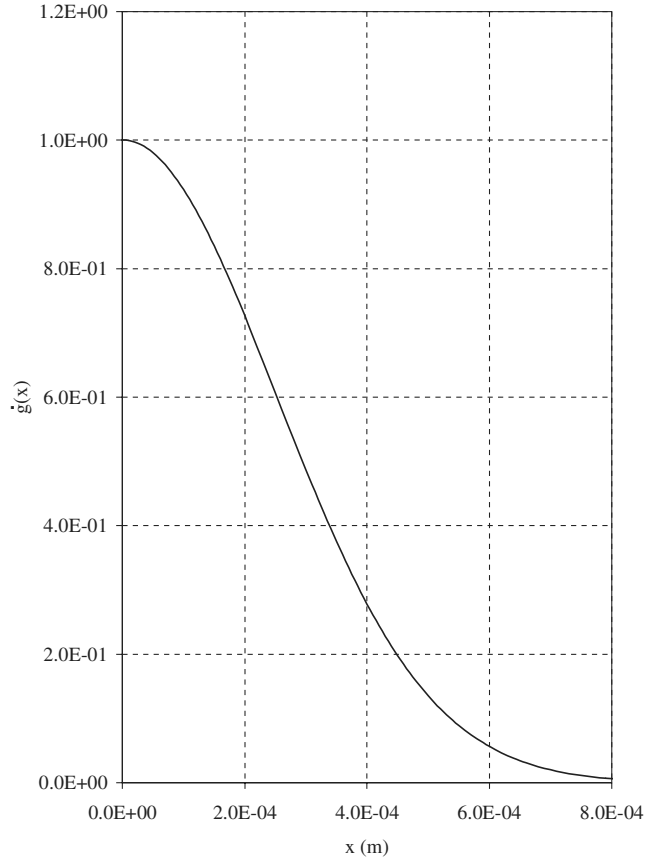

Fig. 3 Spatial function of the laser pulse.

the curve is the same for both lasers. Additional laser beam parameters chosen for this analysis are provided in Table 1.

The slab under consideration loses energy by convection from surfaces 1 and 2. The surfaces at $x = -W$ and $x = W$ are insulated. The boundary conditions at these surfaces can be written as follows:

$$\frac{\partial T}{\partial x} = 0 \quad \text{at} \quad x = -W, W \quad \text{for all} \quad y \tag{6a}$$

$$k\frac{\partial T}{\partial y} = h_1(T - T_\infty) \quad \text{at} \quad y = 0 \quad \text{for all} \quad x, t > 0 \tag{6b}$$

$$-k\frac{\partial T}{\partial y} = h_2(T - T_\infty) \quad \text{at} \quad y = L \quad \text{for all} \quad x, t > 0 \tag{6c}$$

The initial condition is

$$T = T_\infty \quad \text{for all} \quad x \quad \text{and} \quad y \quad \text{at} \quad t = 0 \tag{7}$$

III. Two-Dimensional Integral-Transform Solution

For semi-infinite slabs, the common procedure is to apply the Laplace transform to the partial differential equation and boundary conditions. However, to the best of the authors' knowledge, this technique is not readily applicable for a slab with a finite dimension subjected to a complex internal heat generation term [Eq. (2)] as the inverse transformation does not exist. Instead, it has been established that the integral-transform technique can be used [9]. For simplicity the environment was set at zero temperature ($T_\infty = 0$). A general solution of Eq. (1) has been developed with this technique by Özisik [10] and can be written as

$$T(x, y, t) = \sum_{m=1}^{\infty}\sum_{n=1}^{\infty}\frac{X(\beta_m, x)Y(\gamma_n, y)}{M(\beta_m)N(\gamma_n)}e^{-\alpha(\beta_m^2+\gamma_n^2)t} \times \frac{\alpha}{k}\int_{t'=0}^{t} e^{\alpha(\beta_m^2+\gamma_n^2)t'}\bar{g}(\beta_m, \gamma_n, t')\mathrm{d}t' \tag{8}$$

where

$$\bar{g}(\beta_m, \gamma_n, t') = \int_{x'=0}^{W}\int_{y'=0}^{L} X(\beta_m, x')Y(\gamma_n, y')\dot{g}'''(x', y', t')\mathrm{d}x'\mathrm{d}y' \tag{9}$$

In the preceding equations, boundary conditions are used to determine the eigenfunctions $X(\beta_m, x)$ and $Y(\gamma_n, y)$, the normalization integrals $M(\beta_m)$ and $N(\gamma_n)$, and the eigenvalues β_m and γ_n. The normalization integrals are related to the eigenfunctions in the following forms:

$$M(\beta_m) = \int_0^W [X(\beta_m, x')]^2\mathrm{d}x' \tag{10}$$

$$N(\gamma_n) = \int_0^L [Y(\gamma_n, y')]^2\mathrm{d}y' \tag{11}$$

IV. Solution of the Physical Problem

As mentioned previously, the eigenfunctions, the normalization integrals, and the eigenvalues must be tailored for the applicable boundary conditions. For convective cooling at both surfaces, they are defined in the following manner:

1) For the x direction [10]

$$X(\beta_m, x) = \cos\beta_m x \tag{12}$$

$$\frac{1}{M(\beta_m)} = \frac{2}{W} \quad \text{for} \quad \beta_m \neq 0$$
$$= \frac{1}{W} \quad \text{for} \quad \beta_1 = 0 \tag{13}$$

Eigenvalues $\beta_m = (m-1)\pi/W$ for $m = 2, 3, 4, \ldots$ ($\beta_1 = 0$ is also an eigenvalue corresponding to $X = 1$).

2) For the y direction [10]

$$Y(\gamma_n, y) = \gamma_n \cos \gamma_n y + H_1 \sin \gamma_n y \tag{14}$$

$$\frac{1}{N(\gamma_n)} = \frac{2}{(\gamma_n^2 + H_1^2)(L + \frac{H_2}{\gamma_n^2 + H_2^2}) + H_1} \tag{15}$$

where $H_1 = h_1/k$ and $H_2 = h_2/k$. Eigenvalues γ_n are positive roots of

$$\tan \gamma_n L = \frac{\gamma_n (H_1 + H_2)}{\gamma_n^2 - H_1 H_2} \tag{16}$$

Based on the aforementioned assumptions, boundary conditions, and initial condition, the temperature distribution within the two-dimensional slab is represented in analytical form as

$$\begin{aligned} T(x, y, t) = {} & \frac{\alpha \mu I_o (1 - R)\sqrt{\pi}}{4kb} \sum_{m=1}^{\infty} \sum_{n=1}^{\infty} \frac{X(\beta_m, x) Y(\gamma_n, y)}{M(\beta_m) N(\gamma_n)} \\ & \times \left\{ \frac{[(a - \delta)e^{\delta t} - (a - \theta)e^{\theta t}]e^{(a - \theta - \delta)t} - \theta + \delta}{(a - \theta)(a - \delta)} \right\} \\ & \times \{[(\gamma_n^2 - \mu H_1) \sin \gamma_n L - \gamma_n (\mu + H_1) \cos \gamma_n L] e^{-\mu L} \\ & + \gamma_n (\mu + H_1)\} \left[\operatorname{erf}\left(bW - \frac{\beta_m}{2b} i \right) \right. \\ & \left. + \operatorname{erf}\left(bW + \frac{\beta_m}{2b} i \right) \right] \frac{e^{-\beta_m^2 / 4b^2}}{\mu^2 + \gamma_n^2} e^{-at} \end{aligned} \tag{17a}$$

where i is the imaginary unit and $\operatorname{erf}(x)$ is the error function [12] while

$$a = \alpha(\beta_m^2 + \gamma_n^2) \tag{17b}$$

and

$$b = 2\sqrt{2}/d \tag{17c}$$

As stated previously, the results from the present study will be compared with one-dimensional cases. The one-dimensional temperature distribution is presented herein for reference, Eq. (17). Based on the same assumptions and boundary conditions for surfaces 1 and 2, the temperature distribution for a one-dimensional finite slab takes the form as [9]

$$\begin{aligned} T(y, t) = {} & \frac{\alpha \mu I_o (1 - R)}{k} \sum_{n=1}^{\infty} \frac{Y(\gamma_n, y)}{N(\gamma_n)} \\ & \times \left\{ \frac{[(\alpha\gamma_n^2 - \delta)e^{\delta t} - (\alpha\gamma_n^2 - \theta)e^{\theta t}]e^{(\alpha\gamma_n^2 - \theta - \delta)t} - \theta + \delta}{(\alpha\gamma_n^2 - \theta)(\alpha\gamma_n^2 - \delta)} \right\} \\ & \times \{[(\gamma_n^2 - \mu H_1) \sin \gamma_n L - \gamma_n (\mu + H_1) \cos \gamma_n L] e^{-\mu L} \\ & + \gamma_n (\mu + H_1)\} \frac{e^{-\alpha\gamma_n^2 t}}{\mu^2 + \gamma_n^2} \end{aligned} \tag{18}$$

V. Results and Discussion

An analytical solution for the two-dimensional temperature distribution within a rectangular slab subjected to a realistic laser pulse has been formulated. The solution was in the form of an infinite series and was numerically evaluated in Maple [13] using eigenvalues determined by the appropriate boundary function. Eigenvalues were calculated in Matlab [14] using the bisection and secant root-finding methods in series. The number of eigenvalues needed to evaluate the series solution was found by successively increasing the number of terms until additional terms did not significantly alter the temperature profile. In all cases, at least 100 terms were needed with a greater number required for smaller time scales.

All cases were simulated for a slab of pure silicon using the thermophysical and optical properties: $k = 156$ W/m · K, $\rho = 2330$ kg/m^3, $c_p = 713$ J/kg · K, $\mu = 4952.65$ 1/m, and $R = 0.3186$ [15,16]. Silicon was chosen for the simulations because it is widely used in the semiconductor industry and information on the thermophysical and optical properties was readily available. Unless otherwise noted, all cases were simulated using the laser heating profile of laser 1.

The depth to which laser energy is deposited into the slab was defined by the absorption coefficient. Because the absorption coefficient remained constant in this study, two slab thicknesses were considered, one less than $1/\mu$ and another greater than $1/\mu$. A slab thickness of 0.1 mm (less than $1/\mu$) allowed a portion of the incident energy to be transmitted through the slab, but a slab thickness of 1 mm (much greater than $1/\mu$) caused all of the incident energy to be absorbed within the slab before reaching the opposite side (surface 2).

The convection coefficients were calculated differently for each slab. Each convection coefficient was determined from the appropriate Biot number correlation for the given slab thickness. Because the characteristic length of the 0.1 mm and 1 mm slabs were different, the definition of the Biot number was different for the two slabs. For thin slabs, the Biot number was defined by the characteristic length $L/2$, Eq. (19a). However, for thick slabs, the characteristic length was defined by the inverse absorption coefficient $(1/\mu)$, Eq. (19b) [4]. The change in characteristic length occurs when $L/2$ is greater than $(1/\mu)$; in this case, the slab can be seen as semi-infinite in the y direction,

$$Bi = \frac{hL}{2k} \tag{19a}$$

$$Bi = \frac{h}{\mu k} \tag{19b}$$

The choice of defining the Biot number based on the optical depth of the material remains a point of difficulty when considering convection on surface 2. Whereas the optical depth is a suitable characteristic length of conduction on surface 1, the plate thickness itself might be more appropriate for surface 2. Because cooling effects at the heated surface dominated the shape of the temperature profile in all cases, the optical depth was chosen as the most suitable characteristic length [4–8].

For slab thicknesses greater than 10 times the optical depth of the material, semi-infinite solution techniques may be appropriate. In this case the heating of the material is limited to the side of laser incidence, and cooling at that surface prevents significant conduction of heat to the other side. Modeling the slab in two dimensions offered the ability to study the effect of heat spreading in the in-plane direction.

Temperature distributions in the y direction were evaluated at the center of the slab $x = 0$ for several different times. These data are summarized in Figs. 4 and 5 for slab thicknesses of 0.1 mm and 1 mm, respectively. These graphs show that the peak temperature was located within the slab rather than at the surface. As expected, the difference between the maximum temperature and the surface 1 temperature increased with increasing Biot number and time. The maximum temperature was higher for smaller Biot numbers because there was less convective cooling at the surface; in parallel, the maximum temperature was deeper into the slab for larger Biot numbers because there was more convective cooling at the surface.

The peaks shown for the 1 mm slab are similar in size to those in the 0.1 mm slab, though they appear different due to the scale of the graphs. For the 0.1 mm slab, the laser energy reached surface 2 of the 0.1 mm slab; however, the effect of the laser could not be seen at surface 2 of the 1 mm slab. The cooling effect at surface 2 was different for these two slabs mainly because the attenuated energy was absorbed within the thicker slab before reaching surface 2. For the 0.1 mm slab, there was less energy leaving surface 2 than

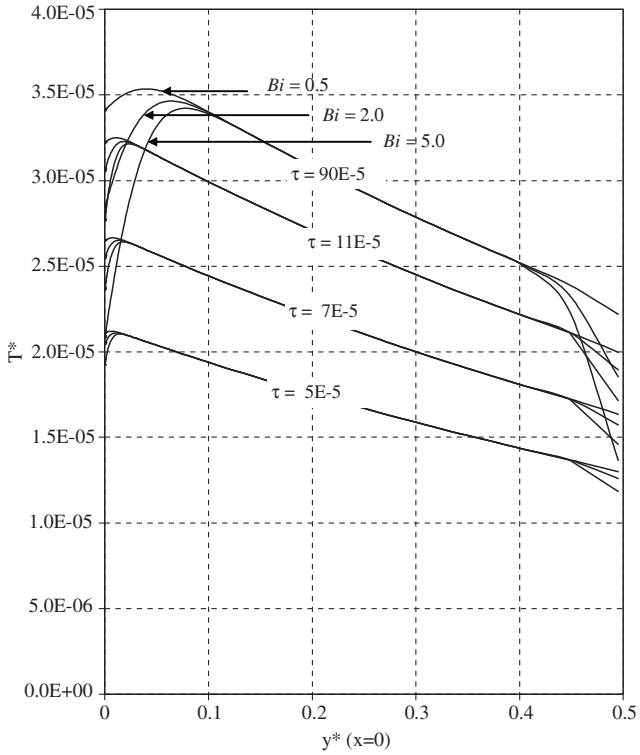

Fig. 4 Dimensionless temperature profile as a function of y^* at $x = 0$ for various Biot numbers and τ (0.1 mm slab).

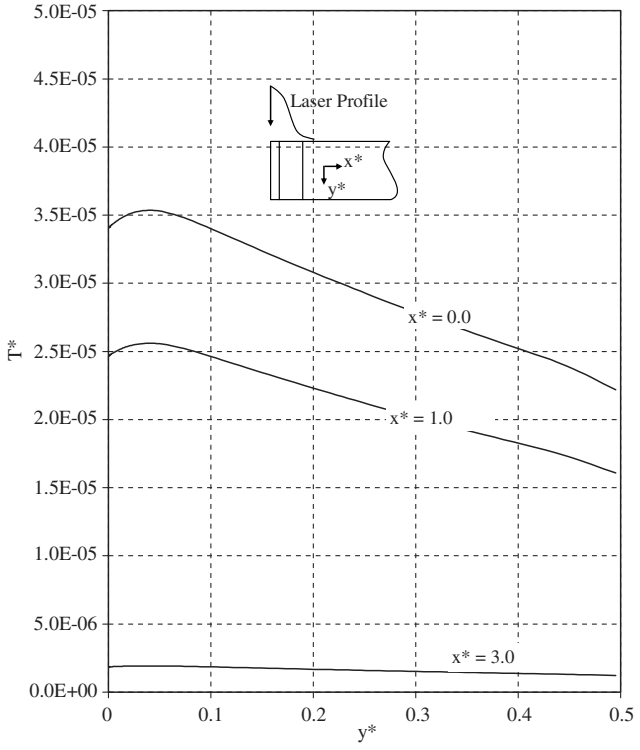

Fig. 6 Dimensionless temperature profile as a function of y^* for $Bi = 0.5$ and $\tau = 90 \times 10^{-5}$ at various x^* values (0.1 mm slab).

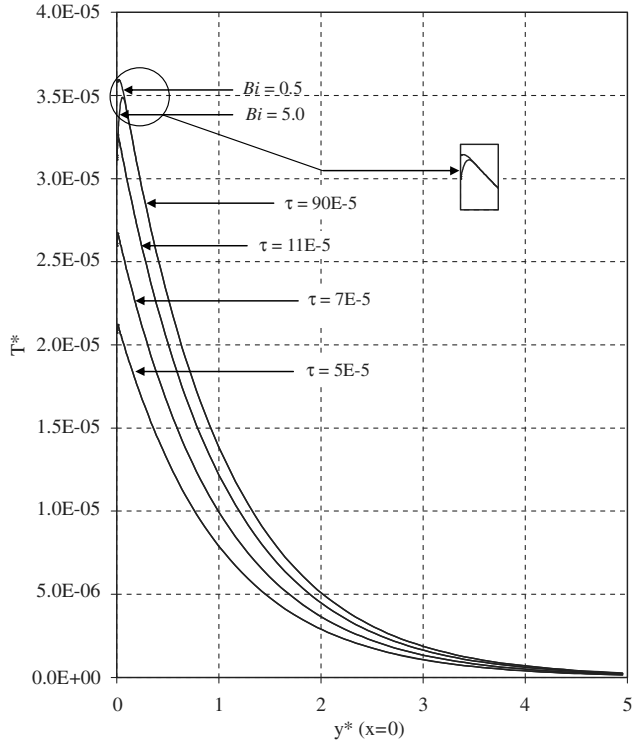

Fig. 5 Dimensionless temperature profile as a function of y^* at $x = 0$ for various Biot numbers and τ (1 mm slab).

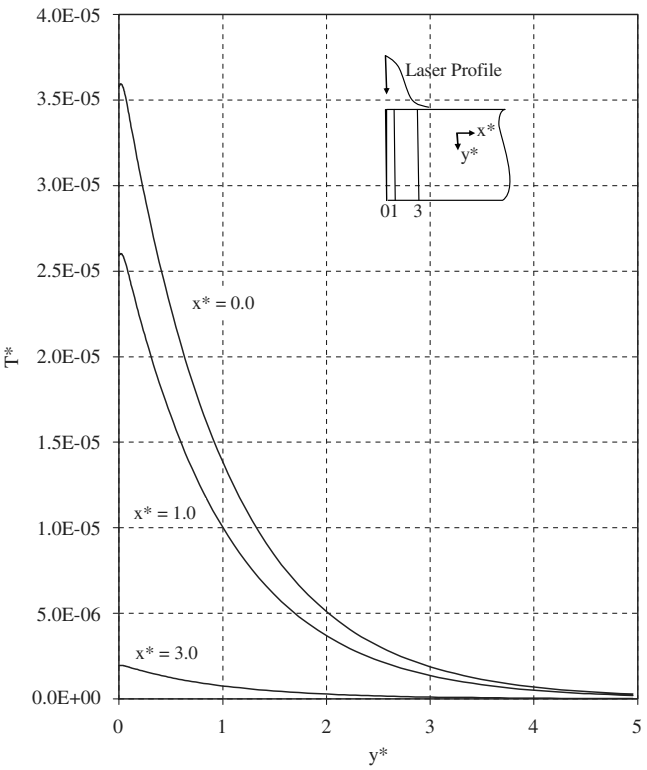

Fig. 7 Dimensionless temperature profile as a function of y^* for $Bi = 0.5$ and $\tau = 90 \times 10^{-5}$ at various x^* values (1 mm slab).

surface 1 because the temperature of surface 1 was higher than the temperature of surface 2.

The temperature distributions in the y direction for different cross sections along the x axis are shown in Figs. 6 and 7. These profiles were taken for $Bi = 0.5$ at a time of $\tau = 90 \times 10^{-5}$. The schematics within Figs. 6 and 7 show the laser profile along the x direction and where the cross sections were taken. Both Figs. 6 and 7 show each temperature profile in the y direction decreasing in magnitude with x because of the Gaussian laser profile.

Temperature distributions in the x direction were evaluated at the surface of the slab ($y = 0$) for several different times. These temperature distributions are shown in Figs. 8 and 9. The temperature profile at each time copied the Gaussian distribution of the laser,

showing an exponential decrease from the center to edge of the laser beam. The beam radius is illustrated on Figs. 8 and 9 as a reference point. Although there was some heat spreading in the x direction, the laser heating had only a small impact on the area outside the beam radius.

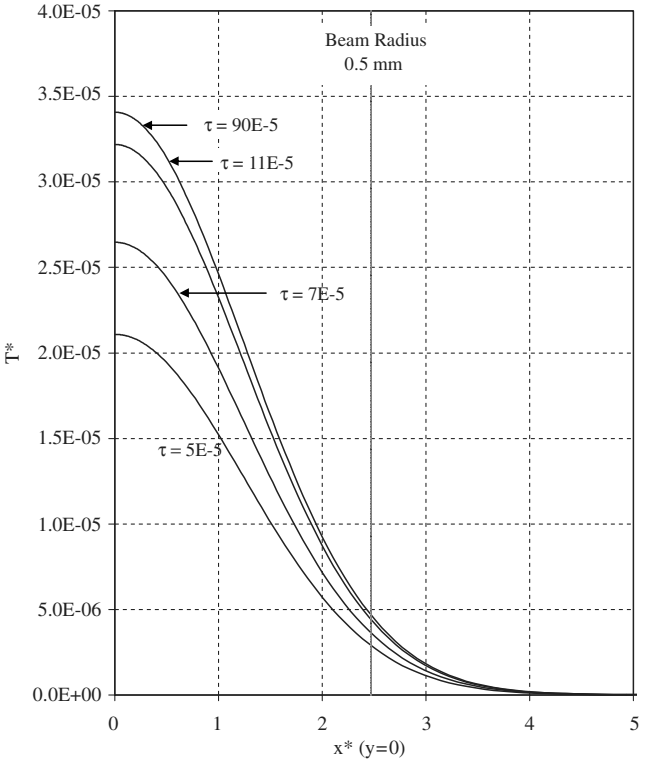

Fig. 8 Dimensionless temperature profile as a function of x^* at $y = 0$ for $Bi = 0.5$ and various τ (0.1 mm slab).

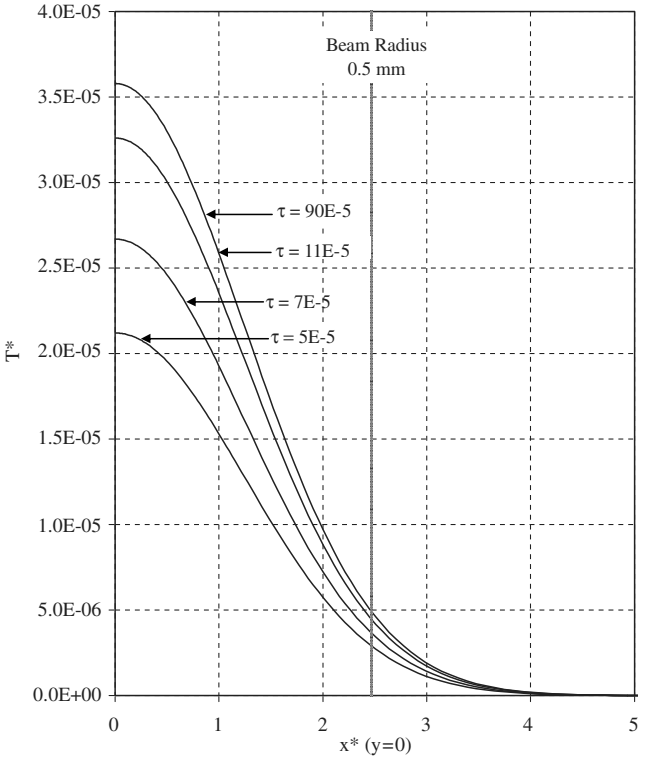

Fig. 9 Dimensionless temperature profile as a function of x^* at $y = 0$ for $Bi = 0.5$ and various τ (1 mm slab).

The temperature distributions in the x direction for different values along the y axis are shown in Figs. 10 and 11. These profiles were taken for $Bi = 0.5$ at a time of $\tau = 90 \times 10^{-5}$. The schematics within Figs. 10 and 11 show the laser profile along the x direction and illustrate the cross sections of the y axis from which the data curves in the graph were taken. In each case, the maximum temperature

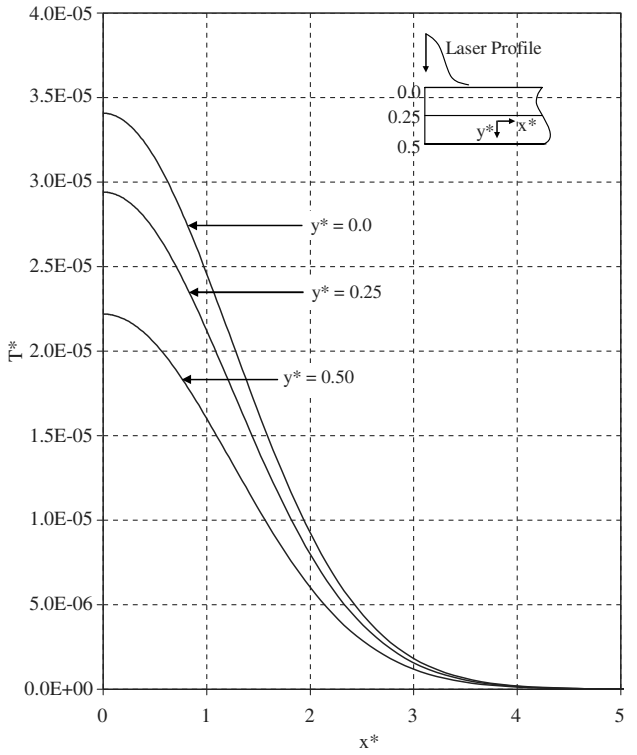

Fig. 10 Dimensionless temperature profile as a function of x^* for $Bi = 0.5$ and $\tau = 90 \times 10^{-5}$ at various y^* values (0.1 mm slab).

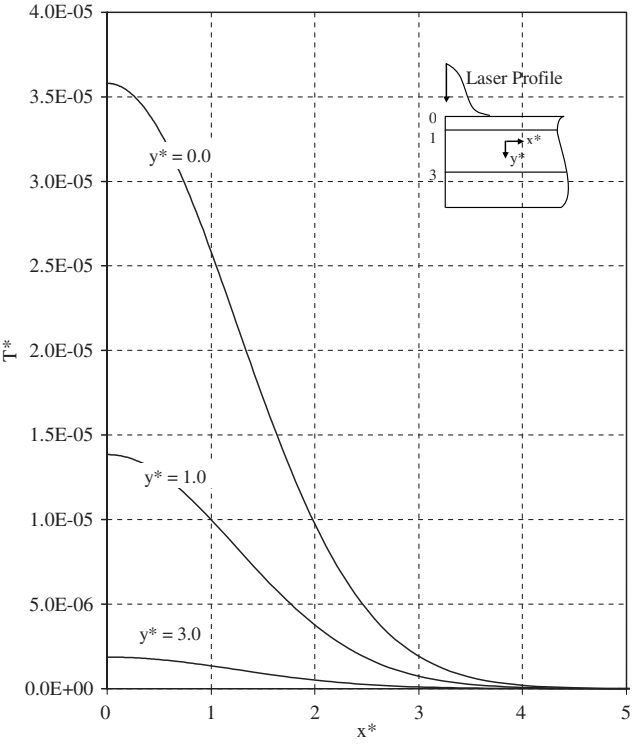

Fig. 11 Dimensionless temperature profile as a function of x^* for $Bi = 0.5$ and $\tau = 90 \times 10^{-5}$ at various y^* values (1 mm slab).

occurred at $x^* = 0$. The temperature profile for each cross section was cooler at greater depths due to a combination of beam attenuation and conduction.

To help further visualize the temperature distribution within the slab, contour plots, shown in Fig. 12 (0.1 mm slab) and Fig. 13 (1 mm slab), were created for $Bi = 5.0$. Essentially, each contour plot illustrates an $x - y$ cross section of the slab at one of four times. The lines in the plots represent isotherms, and the color shading represents the temperature magnitude. Recall that the laser impinged the slab at $x^* = 0$ and $y^* = 0$. Thus, as expected, the slab was hottest near the origin. More interestingly, the progression of the maximum temperature with time could be seen. By $\tau = 90 \times 10^{-5}$, the maximum temperature was located well beneath the surface. It should be noted that only one-fifth of the slab thickness is shown in Fig. 13.

To determine the influence of heat spreading in the in-plane direction, the through-thickness temperature profiles were compared with the temperature profiles determined with a one-dimensional model [9] that only considered heat transfer in the y direction. To maintain consistency between the two models, the same peak power density used. The difference between the one- and two-dimensional results revealed the implicit error in the one-dimensional analysis from neglecting in-plane conduction. Comparisons are shown in Figs. 14 and 15 for two different times ($t = 90 \times 10^{-5}$ and $\tau = 5 \times 10^{-2}$) and for slab thicknesses of 0.1 mm and 1 mm, respectively. As can be seen in both figures, there was only a small difference in temperature for the one- and two-dimensional simulations. The temperature difference was attributed to the effect of in-plane heat spreading.

The two times considered for the comparison were evaluated for $Bi = 0.5$. Based on heat transfer fundamentals, the temperature difference between the one- and two-dimensional cases should be greater for the thicker 1 mm slab; however, because the convection coefficients were determined differently for the two slabs, a direct comparison cannot be made.

In each case, the temperature difference along the y axis between the one- and two-dimensional simulations strongly resembled the through-thickness temperature profiles. This was expected because higher temperatures resulted in larger in-plane gradients that increased lateral conduction. It was determined that the temperature difference increased with temperature. Furthermore, it was discovered that the temperature difference also increased with time. Having said this, the temperature difference as a function of temperature and time can be written as follows:

$$\Delta T^*_{1D-2D} = m(\tau) T^* \tag{20}$$

where $m(\tau)$ represents the change in the temperature difference with time. The dependency of m with time can be seen in Fig. 16.

The contour plots, shown in Figs. 12 and 13, roughly illustrate the movement of the peak temperature with time. To provide a better understanding of the peak temperature progression, a time-resolved temperature trace of the maximum temperature at its corresponding depth is provided for two Biot numbers in Figs. 17 and 18 for slab thickness of 0.1 mm and 1 mm, respectively. Dimensionless time markers have been placed on the graph to provide a sense of how the peak temperature changes with time. In addition, the temperature traces produced by one-dimensional analyses [9], which only considered the through-thickness direction, have been provided for reference.

The peak in each temperature trace represented the highest temperature found within the slab for all time. The time at which this occurred was roughly at the end of the laser pulse. After the laser pulse ended, the depth of the maximum temperature continued to increase as surface 1 was still being cooled by convective heat transfer to the environment. Notice that for the 0.1 mm slab the depth of the maximum temperature reached a limit at $y^*_{T_{max}} \sim 0.25$, halfway through the slab. With equal convection at both surfaces, each surface was cooled until the temperature profile through the slab was symmetrical about $L/2$. For the 1 mm slab, the location of the

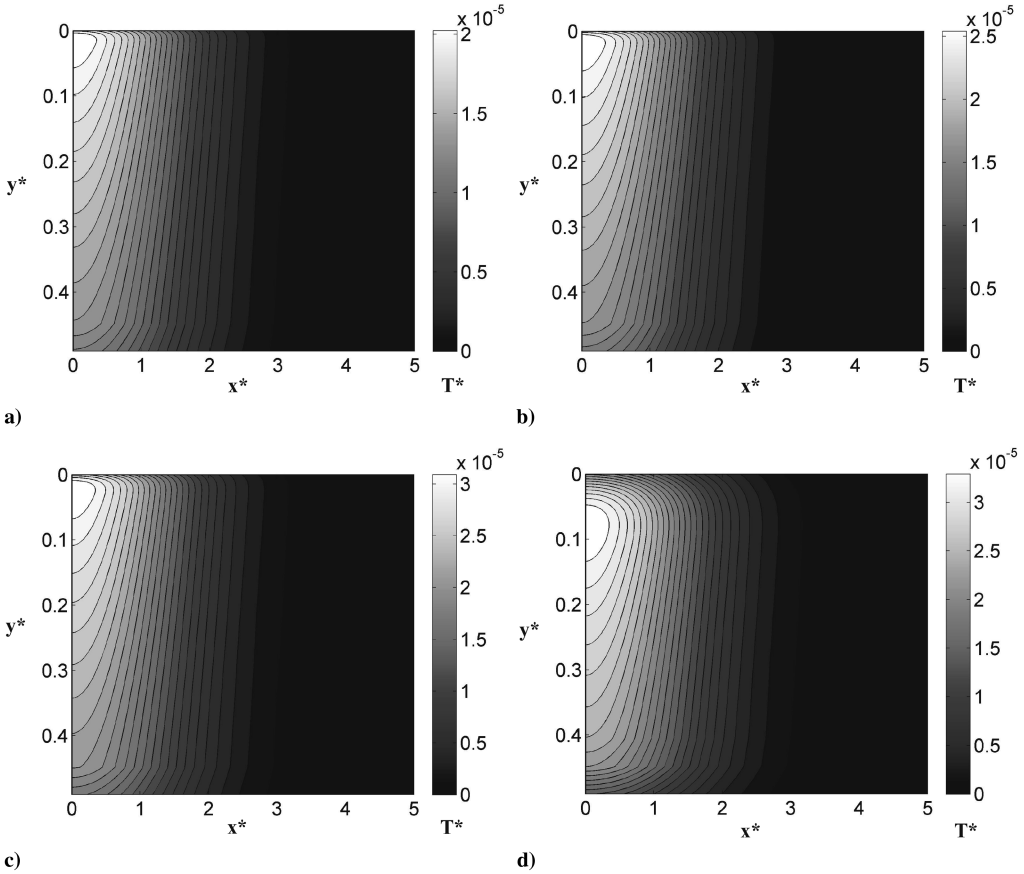

Fig. 12 2-D temperature profile for 0.1 mm slab at a) $\tau = 5 \times 10^{-5}$, b) $\tau = 7 \times 10^{-5}$, c) $\tau = 11 \times 10^{-5}$, and d) $\tau = 90 \times 10^{-5}$.

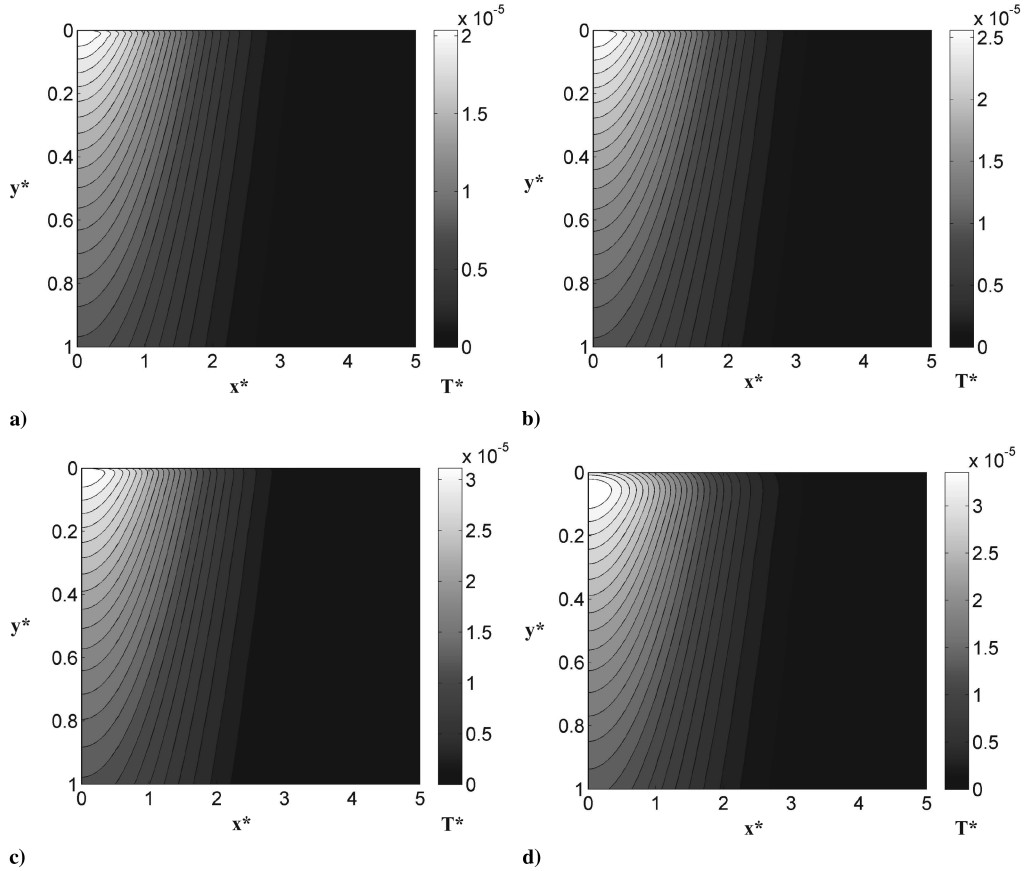

Fig. 13 2-D temperature profile for a 1 mm slab at a) $\tau = 5 \times 10^{-5}$, b) $\tau = 7 \times 10^{-5}$, c) $\tau = 11 \times 10^{-5}$, and d) $\tau = 90 \times 10^{-5}$.

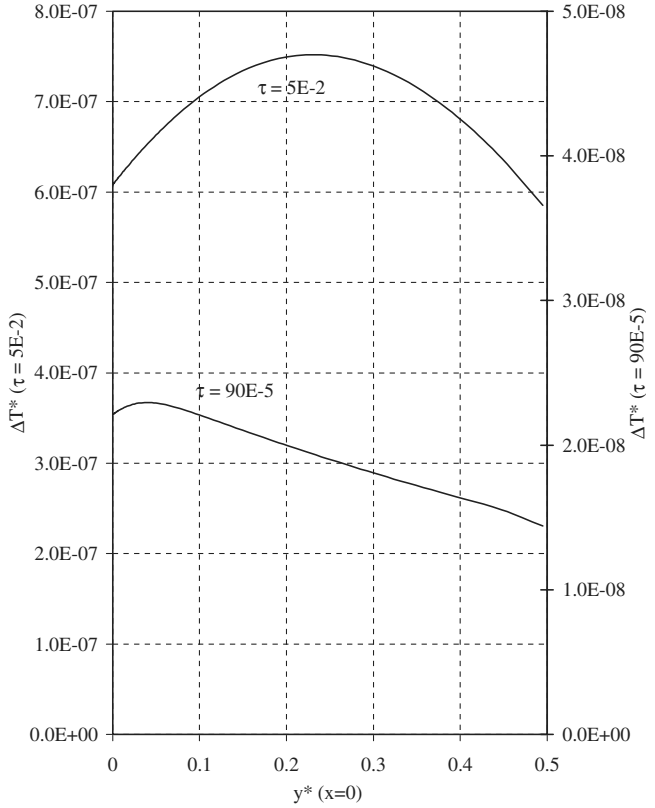

Fig. 14 Temperature difference between 1-D and 2-D calculations for a 0.1 mm slab and $Bi = 0.5$.

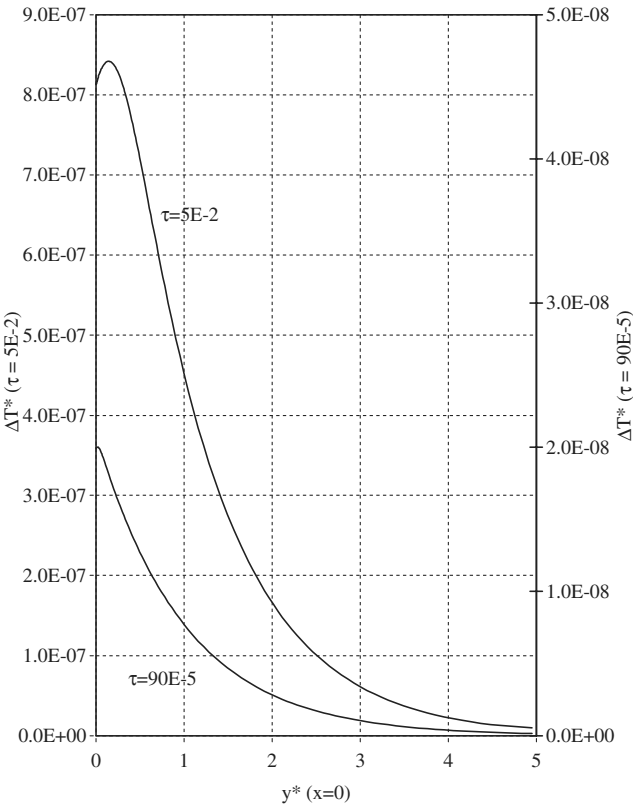

Fig. 15 Temperature difference between 1-D and 2-D calculations for a 1 mm slab and $Bi = 0.5$.

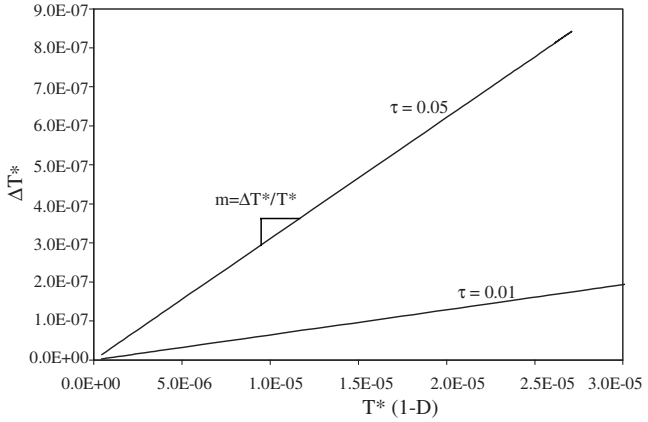

Fig. 16 Temperature difference between 1-D and 2-D calculations as a function of temperature for a 1 mm slab at $\tau = 0.01$ and 0.05.

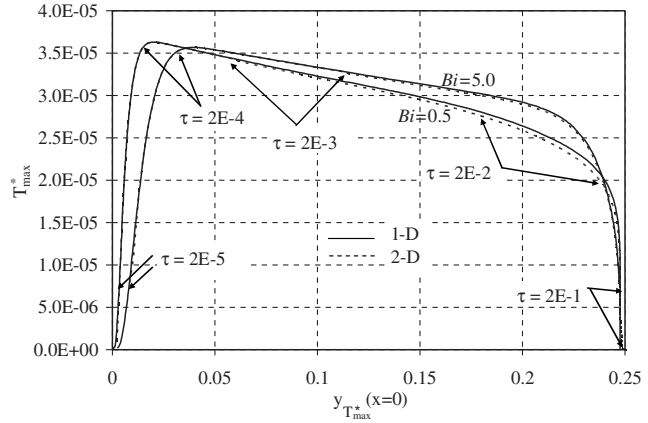

Fig. 17 Dimensionless temperature as a function of depth at which maximum temperature occurs for increasing time intervals (0.1 mm slab).

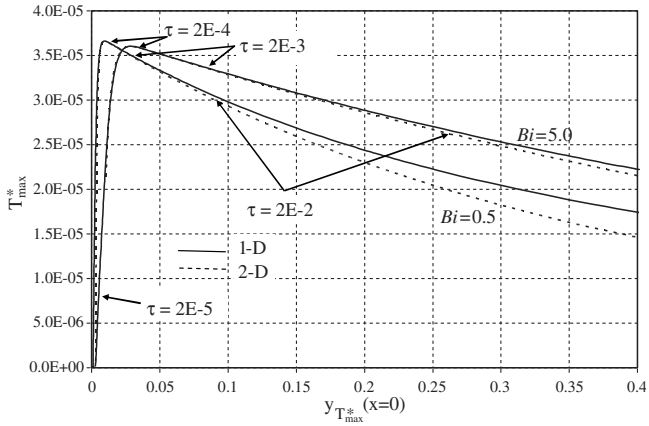

Fig. 18 Dimensionless temperature as a function of depth at which maximum temperature occurs for increasing time intervals (1 mm slab).

maximum temperature continued to travel toward surface 2 because convection played a minimal role at surface 2.

One of the benefits of two-dimensional over one-dimensional analysis was that in-plane conduction was also considered. The effect of in-plane conduction is noticeable in Figs. 17 and 18; with heat spreading in the in-plane direction, the maximum temperature for the two-dimensional analysis was slightly lowered. Furthermore, the effect of heat spreading was greater for smaller Biot numbers because there was less resistance to conduction. Because conduction is a relatively slow process, its impact is more visible at larger times.

Up to this point, all of the calculations were done using the laser profile of laser 1 in Fig. 2 and Table 1. To show the effect of the laser profile on the temperature distribution, results were obtained for laser 2 as well. As mentioned previously, these two laser profiles had the same pulse parameter ratio, buy the peak intensity of laser 2 was half of laser 1. Also the FWHM pulse length of laser 2 was twice as long as laser 1, making the total amount of energy deposited into the slab the same for both lasers. Laser 2 was analyzed for a slab thickness of 0.1 mm, and the results are summarized in Figs. 19 and 20.

For both lasers, the depth of the maximum temperature increased with time; however, Fig. 19 shows that although the same amount of energy was deposited by each laser, the maximum temperature was deeper in the slab for laser 1, which has a higher peak intensity. Even after the laser 2 pulse has ended, approximately $\tau = 4.6 \times 10^{-4}$, the maximum temperature remains deeper for laser 1. Figure 20 shows that the initial nondimensional maximum temperature is also greater for laser 1; however, once the laser 2 pulse has ended, the nondimensional maximum temperature converges for both lasers.

VI. Conclusions

An analytical solution for the two-dimensional temperature distribution within a slab subjected to spatially and temporally decaying laser heating has been developed using the integral-transform technique. Solutions to the problem were obtained for convective boundary conditions at the top and bottom sides of the slab and adiabatic boundary conditions at the remaining sides of the slab. This method can be used to determine the temperature profile within a material sample for a variety of engineering applications. The two-dimensional model improved upon one-dimensional

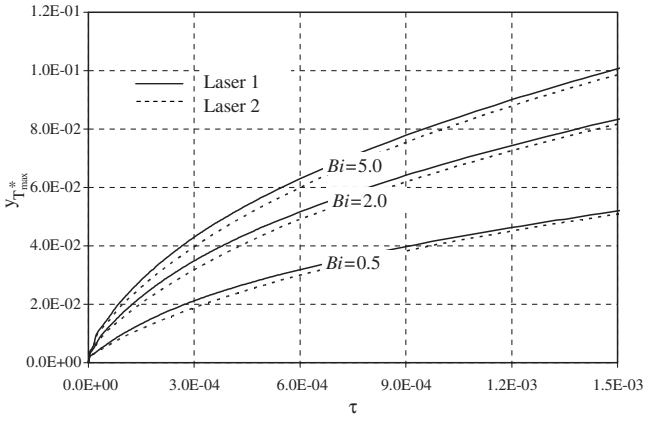

Fig. 19 Dimensionless depth at which maximum temperature occurs for two laser profiles as a function of τ for various Biot numbers (0.1 mm slab).

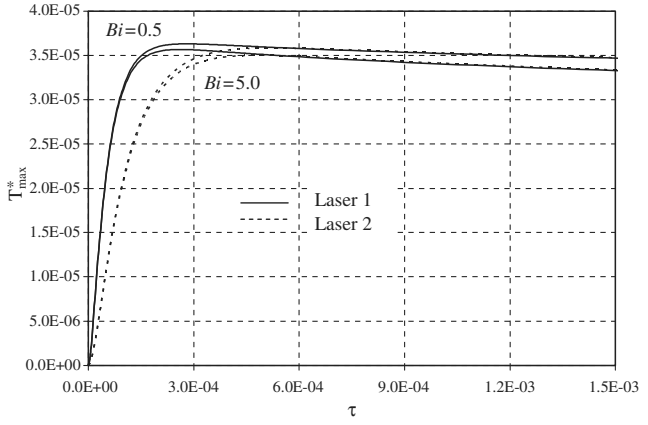

Fig. 20 Dimensionless maximum temperature for two laser profiles as a function of τ for various Biot numbers (0.1 mm slab).

models as well as models limited to semi-infinite media. Furthermore, a more realistic laser pulse function was defined and used in this study. Earlier models in this area dealt mainly with semi-infinite media and constant or decaying laser pulses.

In all cases considered in this work, the point of maximum temperature was observed to be inward from the surface, a result consistent with earlier investigations. Convection at the two surfaces affected the location of the peak temperature over time. As the Biot number associated with either surface was made larger, the prominence of the peak increased with respect to the temperature at the surface of incidence. The effect of cooling at the unheated surface on the temperature profile depended on the ratio of optical depth to slab thickness. When slab thickness was on the order of the optical depth, cooling effects at both surfaces were significant. For slab thicknesses greater than 10 times the optical depth, only cooling at the heated surface played a noticeable role. In such cases a semi-infinite approximation may be appropriate.

When comparing the one- and two-dimensional slab temperature distributions, it was apparent that in-plane spreading, which was simulated in the two-dimensional case, had a noticeable effect on the temperature distribution. As some energy was spread laterally within the slab, the maximum temperature was lower and was not as deep within the slab. In addition, the differences between one- and two-dimensional solutions were shown to be greater for higher temperatures and longer times.

The effect of the laser profile was also demonstrated. Its effect was most apparent for small times. It was demonstrated that lasers with the same pulse parameter ratio, which deposit the same amount of energy, produced different nondimensional temperature profiles. Characterizing the laser pulse profile is important for obtaining the most accurate results.

References

[1] Chen, J. K., Tzou, D. Y., and Beraun, J. E., "Numerical Investigation of Ultrashort Laser Damage in Semiconductors," *International Journal of Heat and Mass Transfer*, Vol. 48, Nos. 3–4, 2005, pp. 501–509. doi:10.1016/j.ijheatmasstransfer.2004.09.015

[2] Metev, S. M., and Veiko, V. P., *Laser-Assisted Microtechnology*, Springer–Verlag, Berlin, 1994, Chap. 4.

[3] Dabby, F. W., and Paek, U., "High-Intensity Induced Laser Vaporization and Explosion of Solid Material," *IEEE Journal of Quantum Electronics*, Vol. 8, No. 2, 1972, pp. 106–111. doi:10.1109/JQE.1972.1076937

[4] Blackwell, B. F., "Temperature Profile in Semi-Infinite Body With Exponential Source and Convective Boundary Condition," *Transactions of the ASME: Journal of Heat Transfer*, Vol. 112, No. 3, Aug. 1990, pp. 567–571. doi:10.1115/1.2910424

[5] Chaudhry, M. A., and Zubair, S. M., "Conduction of Heat in a Semi-Infinite Solid With an Exponential-Type Initial Temperature Profile: Temperature and Heat Flux Solutions Due to an Instantaneous Laser Source," *Wärme- und Stoffübertragung*, Vol. 30, No. 1, 1994, pp. 41–46. doi:10.1007/BF02347002

[6] Zubair, S. M., and Chaudhry, M. A., "Heat Conduction in a Semi-Infinite Solid When Subjected to Spatially Decaying Instantaneous Laser Source," *Wärme- und Stoffübertragung*, Vol. 28, No. 7, 1993, pp. 425–431. doi:10.1007/BF01577884

[7] Zubair, S. M., and Chaudhry, M. A., "Heat Conduction in a Semi-Infinite Solid Due to Time-Dependent Laser Source," *International Journal of Heat and Mass Transfer*, Vol. 39, No. 14, 1996, pp. 3067–3074. doi:10.1016/0017-9310(95)00388-6

[8] Yilbas, B. S., "A Closed Form Solution for Temperature Rise Inside Solid Substrate Due to Time Exponentially Varying Pulse," *International Journal of Heat and Mass Transfer*, Vol. 45, No. 9, 2002, pp. 1993–2000. doi:10.1016/S0017-9310(01)00281-2

[9] Cheung, T. K., Blake, B. A., and Lam, T. T., "Heating of Finite Slabs Subjected to Laser Pulse Irradiation and Convective Cooling," *Journal of Thermophysics and Heat Transfer*, Vol. 21, No. 2, 2007, pp. 323–329. doi:10.2514/1.23100

[10] Özisik, M. N., *Heat Conduction*, 2nd ed., Wiley, New York, 1993, Chaps. 2 and 13.

[11] Ready, J. F., *Industrial Applications of Lasers*, Academic Press, New York, 1978.

[12] Gautschi, W., "Error Function and Fresnel Integrals," *Handbook of Mathematical Functions with Formulas, Graphs, and Mathematical Tables*, 9th edition, edited by M. Abramowitz and I. A. Stegun, Dover, New York, Chap. 7, 1972.

[13] Maple 10, Maplesoft, Waterloo Maple, Inc., Canada, 2005.

[14] Matlab 6.1, The MathWorks, Inc., Natick, MA, 2001.

[15] *Metals Handbook*, American Society for Metals, Vol. 2, American Society for Metals, Materials Park, OH, 1990.

[16] Palik, E. D., *Handbook of Optical Constants of Solids*, Academic Press, New York, 1985.